Received: 26 February 2025 | Revised: 5 May 2025 | Accepted: 22 May 2025

DOI: 10.1111/jmi.13435

Journal of Microscopy RMS

ORIGINAL ARTICLE

Macroscopic and microscopic electron transfer kinetics of HOPG and graphite intercalated compound investigated by cyclic voltammetry and SECM

Rossella Yivlialin[1] | **Gregorio Bonazza**[2] | **Dario Battistel**[3] | **Gianlorenzo Bussetti**[1] | **Salvatore Daniele**[2]

[1]Department of Physics, Politecnico di Milano, Milano, Italy

[2]Department of Molecular Sciences and Nanosystems, Ca' Foscari University of Venice, Venice, Italy

[3]Department of Environmental Sciences, Informatics and Statistics, Ca' Foscari University of Venice, Venice, Italy

Correspondence
Rossella Yivlialin, Department of Physics, Politecnico di Milano, Piazza Leonardo da Vinci 32, 20133 Milano, Italy.
Email: rossella.yivlialin@polimi.it

Dario Battistel, Department of Environmental Sciences, Informatics and Statistics, Ca' Foscari University of Venice, Via Torino 155, Mestre, 30170 Venice, Italy.
Email: dario.battistel@unive.it

Abstract

Highly oriented pyrolytic graphite (HOPG) is one of the most used host materials for obtaining and investigating graphite intercalated compounds, because of the high degree structural order of this polycrystal. Experiments on electrochemically intercalated HOPG in sulphuric acid have a model character, as the results obtained can be usefully generalised, not only with respect to other graphite compounds but also for the intercalation of other layered host lattices. In addition, the HOPG/H_2SO_4 system has an attractive potential for the possibility of electrochemically producing graphite oxide, ideally, by reversible oxidation/reduction cycles, which is of interest for energy storage and graphene production on an industrial scale. However, the oxidation/reduction cycles in such electrochemical intercalation process are not reversible and topotactic, so that the HOPG structure is considerably altered. This alteration may affect, for instance, the quality of the electrochemically produced graphene. In particular, the impact the electrochemical intercalation has on the conductivity of basal planes of HOPG, and so on graphene sheets, is still debated. In this work, we investigated both the macroscopic and microscopic electron transfer (ET) kinetics of the HOPG surface, before and after the intercalation of 1 M H_2SO_4 to obtain graphite intercalated compound, by using cyclic voltammetry (CV) and scanning electrochemical microscopy (SECM), respectively. The heterogeneous kinetic constant (k^0) of the HOPG was evaluated quantitatively by using the redox systems $[Fe(CN)_6]^{3-/4-}$ and $[Ru(NH_3)_6]^{3+/2+}$. The morphology of the samples was also investigated by atomic force microscopy (AFM), which revealed a widespread formation of blisters and precipitates during the HOPG intercalation process. The CV and SECM results indicate that, upon intercalation, the electrochemical behaviour of the HOPG changes sensibly and the ET decreases sensibly. However, this effect depends on the redox mediators employed and it results more dramatic for the $[Fe(CN)_6]^{3-/4-}$ system, for which a decrease of k^0 by orders of magnitude was obtained. The decrease of ET can be correlated to the blisters

and precipitates, which occur during the HOPG intercalation, as observed by AFM.

KEYWORDS
AFM, GIC, HOPG, intercalation, SECM

1 | INTRODUCTION

Intercalation in graphite consists in a charge transfer reaction between electron donors or acceptor species (termed intercalants) and the layers of graphite. The intercalants accommodate in the interlayer spaces of graphite and lead to the expansion of the inter-sheet distance.[1–4] The charge transfer complex with graphite obtained in this reaction is called graphite intercalated compound (GIC).[5] Due to the dual nature of GICs, which can act as donor-type or acceptor-type materials,[2] GICs have been used in many applications, since the middle of the XIX century. Examples include electrical wiring[6] and rechargeable metal-ion batteries,[7] oxide-mixed super-conductors[8] and graphene production by exfoliation.[9] HOPG is one of the most used graphite host for obtaining GIC, given its well-ordered crystalline structure. Many efforts have been made to improve the conductivity of lamellar compounds, formed by the intercalation of pure acids in HOPG, as potential conductors of electricity.[5,10,11] Even more attractive has been the high 2D character of these compounds, in which the intercalants reduce the interplanar coupling in the HOPG and ease delamination into isolated graphene sheets.[12–15] Understanding whether the intercalated HOPG can be considered as the parallel contribution of relatively independent doped graphene sheets and interpreting the phenomenology at the graphite/graphene boundary in terms of in-plane conductivity properties are still challenging.[8,16] The expansion along the *c*-axis of HOPG layers, due to the intercalation of ions in the interlayer spaces, is already known to affect the conductivity of the HOPG basal plane; more specifically, many studies in the past investigated the relative increase of the in-plane conductivity with respect to the conductivity along the *c*-axis of HOPG as a consequence of its intercalation by donor or acceptor species. Those studies were intended to demonstrate, by measuring the properties of the whole crystal, that conductivity of the intercalated HOPG increases to values comparable to the ones in copper.[2,17–19] However, considering the staging process to create GIC, conductivity properties of the intercalated HOPG crystal can be more complex. In fact, according to Hathcock–Murray model,[20,21] the intercalation of species, typically solvated anions, leads to formation of graphene oxide in between the layers, whose impact on the in-plane conductivity, especially of the surface layer of HOPG, has not been clarified yet. In addition, some of the authors demonstrated that during the intercalation step, the surface layer itself is involved in different oxidation processes, which strongly modify the morphology[22,23] and, possibly, the conductivity. The possibility to exchange charges from the surface of intercalated HOPG and the environment (e.g., liquid solutions), and the kinetics with which it occurs must be investigated in view of applications of 2D products obtained from intercalated HOPG (e.g., graphene) in electronic or storage devices.[14,24,25] For this reason, a direct measurement of the in-liquid charge transfer from the surface of 2D source materials is a fundamental preliminary step. To this aim, scanning probe microscopies techniques are useful and, among others, scanning electrochemical microscopy (SECM) can provide direct information on conductivity/reactivity of the sample surfaces.[26–28]

Scanning electrochemical microscopy (SECM) is a contactless scanning probe technique, in which a microelectrode (tip diameter ≤ 25 μm) is used as the probe.[26,27] The microelectrode is connected to piezoelectric elements or step motors to precisely control the probe position in the *x*-, *y*-, and *z*-directions, in proximity of a substrate immersed in a solution. Typically, in SECM operations, a faradaic current, generated at the SECM probe from the electrochemical conversion of a free-diffusing species (i.e., redox mediator), is recoded as a function of the tip-to-substrate distance. The current is modulated by the presence of the substrate and depends on the topography, conductivity and chemical reactivity of the substrate itself [see Section S1 of Supporting Information (SI) for further details].[26] Because of these characteristics, SECM has found application on a variety of fields,[29] including biology,[30,31] catalysis,[32,33] corrosion,[34] sensors,[35] and energy storage systems.[36] In the latter field, SECM has been employed to characterise the performance of anodes and cathodes of metal-ion batteries and accumulators during intercalation/de-intercalation processes of the metal ions. Related techniques, such as scanning electrochemical cell microscopy and combined scanning electrochemical microscopy-atomic force microscopy (SECM-AFM) have been successfully employed to investigate the local surface

electron transfer (ET) of pristine HOPG crystals, of different grades, to elucidate the electrochemical behaviour of basal planes and edges.[37,38] Instead, relatively less attention has been devoted to the investigation of the local surface EC behaviour of intercalated HOPG.

Herein SECM, supplemented by cyclic voltammetry (CV) and AFM measurements, is employed to explore the surface conductivity and EC activity of HOPG samples subjected to EC anion intercalation from the basal plane, performed in sulphuric acid solutions. GICs produced in such a way typically afford to topographic changes, which can be responsible for the decrease of surface conductivity. However, this effect seems somewhat related to the redox system employed to characterise GICs. Therefore, for HOPG materials, the choice of the redox mediator plays a relevant role in the determination of their surface characteristics. Here, the two redox mediators, $Ru(NH_3)_6Cl_3$) and $K_4[Fe(CN)_6]$, which are often employed to investigate the electrochemical behaviour at solid-solution interface,[37,38] are used in the measurements. The SECM approach, having resolution in the order of tens of microns, allowed to identify variations and local changes in activity of the surfaces, expressed as heterogeneous electron transfer rate.

2 | MATERIALS AND METHODS

2.1 | Chemicals and samples

Hexaammine ruthenium (III) chloride ($Ru(NH_3)_6Cl_3$), potassium ferrocyanide $K_4[Fe(CN)_6]$, potassium chloride (KCl), sulphuric acid (H_2SO_4), purchased from Sigma-Aldrich, were of reagent grade and used as received. All aqueous solutions were prepared using Milli-Q water. A diluted (1 M) H_2SO_4 electrolyte was prepared and deaerated by argon bubbling in a separate flask for several hours.

The EC anion intercalation was conducted on (20 × 20 × 1) mm^3 sized HOPG ZYH (i.e., with 3.5°±1.5° mosaic spread) crystals from Optigraph GmbH, previously exfoliated along the 20 mm edge by using an adhesive tape. For more details, see Figure S1 of SI.

2.2 | Instrumentation and electrodes

The intercalation process was performed using a 5500 Keysight Technology EC-AFM instrument, which allowed performing both cyclic voltammetry (CV) and AFM measurements. The EC cell in Teflon was mounted on top of the HOPG surface, which was used as a working electrode (WE); an O-ring created a seal against leaks of the liquid solution. A Pt coil, placed along the wall of the cell, was used as a counter electrode (CE), and another Pt wire was used as a *quasi*-reference electrode (PtQRef). The latter showed adequate stability (down to 10 mV) and in 1 M H_2SO_4 displayed a potential of + 0.52 V versus Ag/AgCl, (KCl saturated) electrode. AFM images were acquired in tapping-mode and in attractive regime, with silicon tips from Bruker (cantilever spring constant: 37 N/m; ν_0 = 320 kHz) and using scan rates of about 1.5 Hz. Once intercalated, the liquid was removed from the EC cell and the samples were dried with nitrogen for the ex situ measurements by AFM. After that, the HOPG samples were moved into another EC cell, to perform both CV and SECM measurements.

SECM and CV experiments were performed using a CHI920C workstation (CH instruments, USA) and an EC cell in Teflon, assembled in the three-electrodes configuration (Figure S3 of SI). The HOPG samples were immobilised at the bottom of the cell by an O-ring (thus leaving a circular surface area of ∼0.079 cm^2 (as defined by the inner O-ring diameter) in contact with the solution. For CV and SECM measurements, the RE and CE were an Ag/AgCl (KCl saturated) and a Pt wire, respectively. In SECM measurements, Pt microelectrodes were used as SECM tips. They were prepared by a standard procedure, by sealing platinum wires of 25 μm in diameter into glass capillaries.[26,27] The tip ends were tapered to a conical shape, such that the overall tip radius (R) to microdisk electrode radius (a) ratio (i.e., $RG = R/a$)[26] was comprised in the range 5–10. Prior use, the microdisks were polished with graded alumina powder of different sizes (1, 0.3 and 0.05 μm) on a polishing microcloth.

The effective radius of the tip was determined from the steady state limiting current ($I_{T,inf}$) recorded in the bulk solution of 1 mM $[Ru(NH_3)_6]Cl_3$ in 0.1 M KCl, by using Equation (1):[39]

$$I_{T,inf} = 4n\ F\ D\ C^b\ a, \tag{1}$$

where n is the number of electrons, D is the diffusion coefficient (for $[Ru(NH_3)_6]^{3+}$, $D = 7.0\times10^{-6}$ cm^2 s^{-1}),[40] C^b is the bulk concentration. The RG value of the SECM tip was evaluated by fitting experimental and theoretical SECM normalised current (i.e., $I_d/I_{T,inf}$, where I_d is the current recorded at the tip-to-substrate distance, d) against normalised tip-to-substrate distance ($L = d/a$) plots (so called approach curves, Section S1 of SI).[26]

Unless otherwise stated, all SECM measurements were performed in air-saturated aqueous solutions and at room temperature (23± 1°C). Furthermore, the HOPG samples were either kept unbiased or were biased at different potentials, as discussed in detail in Section 3.3.

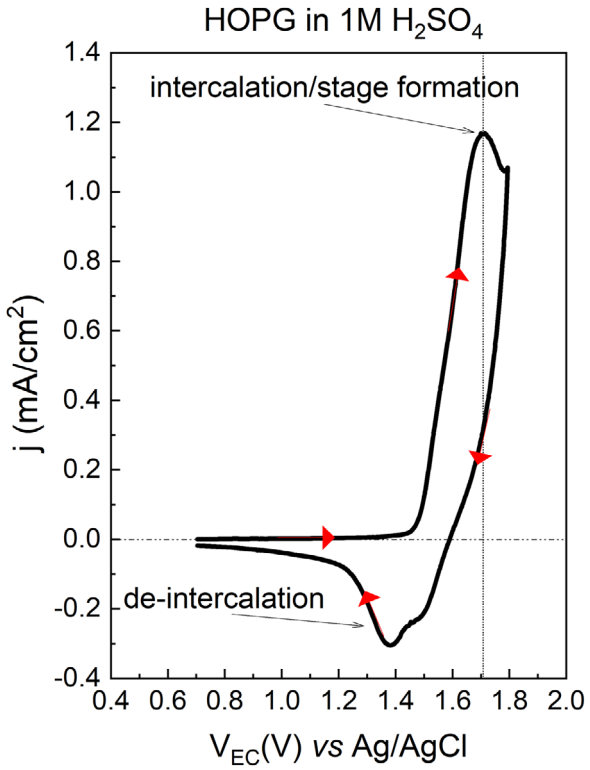

FIGURE 1 Typical voltammogram recorded at 25 mV s^{-1} on HOPG sample immersed in 1 M H_2SO_4 solution. The red arrows indicate the direction of the potential sweep.

3 | RESULTS AND DISCUSSION

3.1 | Intercalation process and surface characterisation by AFM

A HOPG sample was intercalated by performing CVs, using a procedure reported previously.[41] In brief, a freshly exfoliated HOPG crystal was used as the WE in the EC cell containing 1 M H_2SO_4 solution. The intercalation of anions was activated over the potential range 0.7–1.8 V versus Ag/AgCl at 25 mV s^{-1}, and a typical voltammogram recorded is shown in Figure 1. Here, the anodic peak at 1.7 V is due to the occurrence of intercalation of 'guest' anions such as solvated HSO_4^- and SO_4^{2-} into the interlayer spaces of graphite (i.e., GIC formation).[20] Alternation of occupied/unoccupied layer gaps by the solvated anions in the graphite crystal forms a regular array, called 'stage'. Together with the stage formation, at potential values higher than 1.5 V, the relatively low concentration of the acid in the system induced side reactions such as the production of O_2, CO_2 and CO, the effect of which on the graphite crystal will be discussed below. Also, due to the overoxidation process, intermediate compounds such as acid graphite salts undergo a partial hydrolysis to electrochemically(produced) graphite oxide (i.e., EGO).[1] According to this, the peak recorded at about 1.4 V in the cathodic scan of the CV is commonly assigned to both the processes of partial reduction of EGO and partial de-intercalation of anions.[23,42]

Worthy of note is that all the reactions occurring in the anodic scan of the CV are not completely reversible, as can be inferred by the fact that the cahodic to anodic charge ratio involved in the peaks of Figure 1 is much larger than 1. This result is consistent with previous voltammetric investigations of HOPG in various acid electrolytes.[21]

The intercalated HOPG sample was examined ex situ by AFM and Figure 2A,B shows the morphology of the HOPG surface, before and after the voltammetric treatment, respectively. The pristine HOPG surface (panel A) is flat and covered by steps with well-defined and sharp edges (see the cross-section along the white dashed line), in accordance with previous reports.[43] After the intercalation process, the surface strongly modifies, because of all the not fully reversible reactions occurring in the anodic scan of the CV.[43,44] In particular, the surface of HOPG crystals, which have undergone the intercalation in sulphuric acid, typically shows three main discernible morphological features: (1) faceting, due to carbon dissolution starting from the early stages of intercalation and visible on the nanoscale[22] and (2) bubble-like bumps, known as blisters,[20,21] with characteristic dimensions of tenths of nanometres in height and from hundreds of nanometres to few microns in width. An example of blister is shown in the inset of Figure 2C, where the cross-section, plotted in the 1 μm scale (horizontal dashed line), shows the characteristic rounded profile, about 15 nm high and 800 nm wide.

Blisters, as local swellings of the graphite uppermost layers, origin from the gases produced by the EC chemical reaction between intercalants and carbon planes, and are trapped within the interlayer spaces of the graphite crystal. More details about structure, time-formation and mechanics have been widely discussed elsewhere.[45,46]

Precipitates with various sizes and irregular shapes (see the cross-section shown in inset of Figure 2B) are also formed, whereof the origin and composition are not clearly understood, although certainly different from the ones of blisters.[41] Precipitates are observed on the HOPG surface only after removing the solution from the cell and drying the EC-treated sample. They are conceivably due to the hydrolysis of graphite acid salts to EGO (during the overoxidation process)[47] or to the accumulation of carbon compounds originated from the dissolution of the HOPG surface during the CV.[48] In this regard, noteworthy is the (5×5) μm^2 phase image shown in Figure 2D, in which the indication of different mechanical properties and chemical compositions between blisters and precipitates is clearly pointed out by the colour contrast: that is, blue for

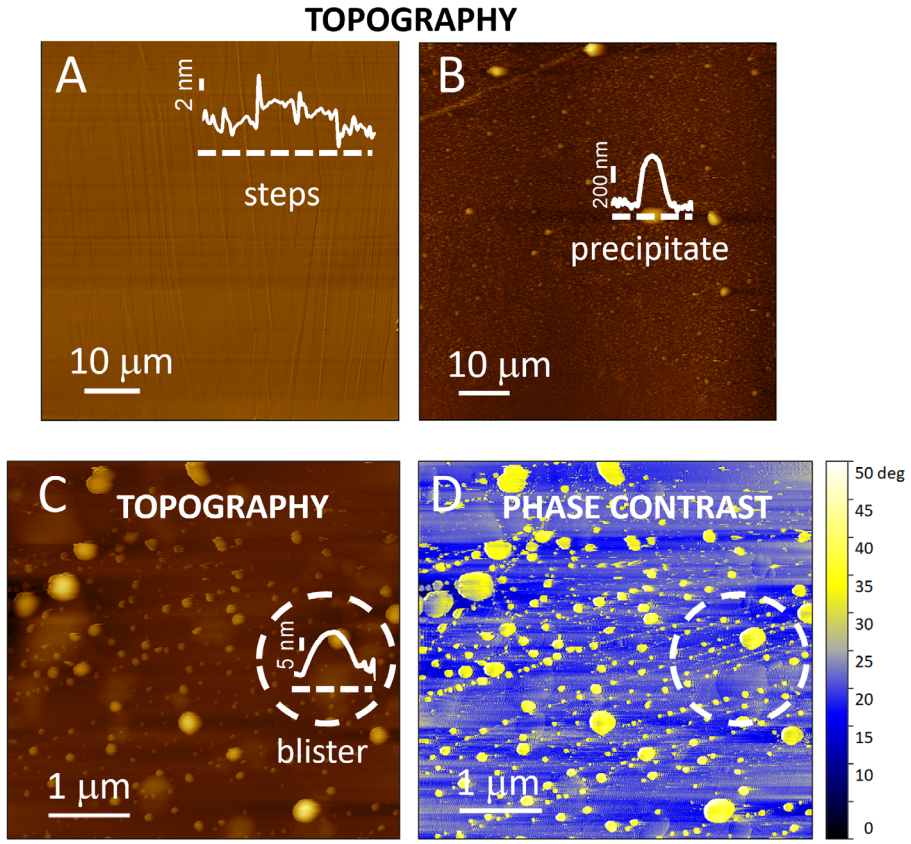

FIGURE 2 Topography AFM images [(80 × 70) µm2] of the HOPG surface immersed in 1 M H_2SO_4, in pristine conditions (A), and after the CV treatment (B); insets show cross-sections of steps and precipitates, respectively, acquired along the horizontal white dashed lines. Topography (C) and the phase contrast signals (D) acquired on a smaller [i.e., (5 × 5) µm2] area of the HOPG surface after the CV treatment; inset in C shows the cross-section of a blister, acquired along the horizontal white dashed line. The white rims (dashed line) mark the blister and some precipitates, visible in both the topography and the phase contrast image. The false colour ruler in D is a guide towards the phase contrast between blisters (in blue) and precipitates (in yellow).

blisters and yellow for precipitates (see, in particular, the area marked by the white rim). It can be anticipated that both blisters and precipitate, conceivably, affect the conductivity/ reactivity of the GIC surface, as will appear from the CVs and SECM results (vide infra).

3.2 | Voltammetric characterisation

Preliminarily, pristine HOPG samples were characterised by cyclic voltammetry using the redox mediators $[Ru(NH_3)_6]^{3+}$ and $[Fe(CN)_6]^{4-}$, which behave as outer-sphere redox probes,[49] and are widely used to characterise HOPG materials.[37,38] Typical CVs recorded at 50 mV s^{-1} at a just exfoliated HOPG sample are shown in Figure 3 (black lines in panels A and B). At this and lower scan rates, both redox mediators displayed an appreciable reversibility, as was verified by the peak-to-peak potential separation (ΔE_p) which were 60 (± 1) mV and 65 (±1) mV for $[Ru(NH_3)_6]^{3+/2+}$ and $[Fe(CN)_6]^{3-/4-}$, respectively. These ΔE_p values are close to the theoretical value of 59 mV, predicted for a one reversible electrode process, and suggest rather fast kinetics.[50]

The voltammetric behaviour changed markedly when the measurements were performed using the GIC sample. In fact, as is shown in Figure 3 (coloured lines panels A and B), the current-potential profiles became more drawn out, ΔE_p increased and depended on the scan rate (Table 1). In addition, at the same scan rate (i.e., 50 mV s^{-1}), both forward and backward peak currents decreased. The above effects were more dramatic for the $[Fe(CN)_6]^{3-/4-}$ system. These results indicate that the activity of GIC is reduced compared to pristine HOPG. Based on ΔE_p values shown in Table 1, the electrode processes at the GIC sample can be classified as totally irreversible for $[Fe(CN)_6]^{3-/4-}$ and *quasi*-reversible for $[Ru(NH_3)_6]^{3+/2+}$.[50]

The analysis of potential parameters of the CVs of the type shown in Figure 3 allowed obtaining information on ET kinetics, in terms of heterogeneous rate constant (k^0, cm s^{-1}) for the two redox probes. In particular, the Nicholson and Shain approach (Equation 2),[51] extended by Lavagnini et al.[52] and Kingler et al.[53] (Equation 3), was

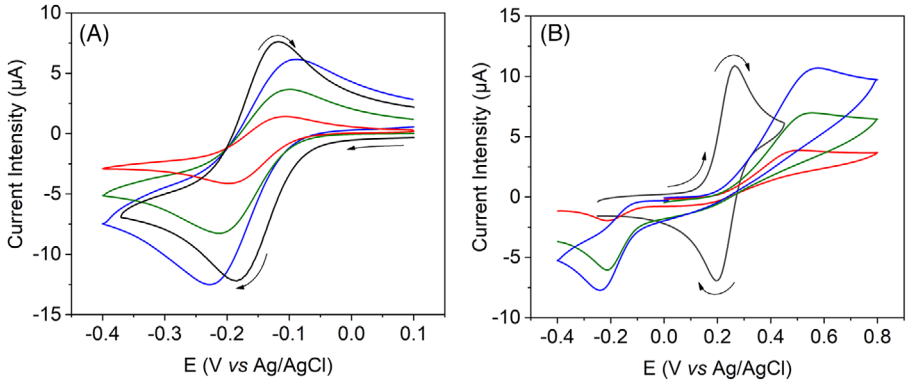

FIGURE 3 Cyclic voltammograms recorded in a solution containing (A) 1 mM $[Ru(NH_3)_6]^{3+}$ + 0.1 M KCl and (**B**) 1 mM $[Fe(CN)_6]^{4-}$ + 0.1 M KCl. The measurements were performed using a HOPG substrate at a scan rate of 50 mV s^{-1} (black line), and a GIC substrate at 5 mV s^{-1} (red line), 20 mV s^{-1} (green line), and 50 mV s^{-1} (blue line).

TABLE 1 Voltammetric parameters obtained from replicate CVs,[a] as those shown in Figure 3A,B.

Redox mediator	Scan rate (mv s^{-1})	Surface	$E_{p,c}$(V)	$E_{p,a}$(V)	ΔE_p(V)	$E_{1/2}$(V)
$[Fe(CN)_6]^{4-}$	50	HOPG	0.195	0.260	0.065	0.228
$[Fe(CN)_6]^{4-}$	50	GIC	−0.240	0.565	0.805	[b]
$[Fe(CN)_6]^{4-}$	20	GIC	−0.210	0.536	0.746	[b]
$[Fe(CN)_6]^{4-}$	5	GIC	−0.200	0.511	0.712	[b]
$[Ru(NH_3)_6]^{3+}$	50	HOPG	−0.181	−0.121	0.060	−0.151
$[Ru(NH_3)_6]^{3+}$	50	GIC	−0.227	−0.089	0.138	−0.158
$[Ru(NH_3)_6]^{3+}$	20	GIC	−0.211	−0.106	0.105	−0.159
$[Ru(NH_3)_6]^{3+}$	5	GIC	−0.192	−0.115	0.077	−0.153

[a]The values refer to at least three replicates and are within ± 10 mV error. $E_{p,c}$ and $E_{p,a}$ correspond to the cathodic and anodic peak potential, respectively. $E_{1/2}$ is the half-wave potential, obtained as $(Ep_a + Ep_b)/2$,[50] using the CVs for reversible or quasi reversible redox systems.
[b]$E_{1/2}$ cannot be determine as indicated above for irreversible electrode process.

used to estimate k^0 values for CVs having ΔE_p in the range 0.065–0.200 V, by using Equations (2) and (3):

$$\psi = k^0 \times \left(\frac{D_R}{D_P}\right)^{\frac{\alpha}{2}} \left(\frac{RT}{\pi n D_R F}\right)^{0.5} \times \upsilon^{-0.5}, \quad (2)$$

$$\psi = \frac{-0.6288 + 0.0021 \times n \times \Delta E_p}{1 - 0.017 \times n \times \Delta E_p}. \quad (3)$$

For the $[Fe(CN)_6]^{3-/4-}$ system at the GIC surface, in which ΔE_p was larger than 0.200 V, the relationship (4), which holds for a totally irreversible system, was employed:[50]

$$I_{p_a} = 0.227FA\, C^b k^0 e^{-\left[\alpha \frac{F}{RT}\left(E_p^a - E^{0'}\right)\right]}. \quad (4)$$

The symbols in the above relationships have the following meaning: ψ is a dimensionless parameter linked to ΔE_p, D_R and D_P are the diffusion coefficients of the reagent and product of the electrode reaction, respectively; α is the transfer coefficient; n is the number electrons (in our cases $n = 1$); v is the scan rate; F and R are the Faradaic and gas constant, respectively; T is the temperature (in Kelvin); I_{p_a} and E_p^a are the anodic peak current and peak potential, respectively; A is the surface area of the investigated sample; C^b is the concentration of the electroactive species in the bulk solution; $E^{0'}$ is the formal potential (here assumed to be equal to the half-wave potential, $E_{1/2}$; see Table 1).[50]

The above equations were not used in the case in which ΔE_p was lower than 63 mV, as they are very close to the reversible limit, and would not provide meaningful k^0 values. This was the case for the CVs obtained for the $[Ru(NH_3)_6]^{3+/2+}$ system at the HOPG sample.

Table 2 (first column) shows kinetic parameters for the two redox systems at the pristine and intercalated HOPG samples. These values are, in general, consistent with literature reports of pristine HOPG or a variety of graphite samples subjected to chemical or electrochemical treatments.[37,54–57] In particular, using the $[Fe(CN)_6]^{3-/4-}$ redox couple, k^0 values were found to vary over several orders of magnitude (i.e., 10^{-9} to 1 cm s^{-1}) for the $[Fe(CN)_6]^{3-/4-}$ system at various types of HOPG. [38] In most of earlier works,[49] these inconsistencies were attributed to the poor electrode kinetics of basal plane compared to step-edges.[37,54–57] However, more recently,

TABLE 2 $k^{0'}$ (cm s^{-1}) values obtained with the two redox mediators at the HOPG and GIC substrate by CV and SECM.

	CV		SECM	
Redox system	**HOPG**	**GIC**	**HOPG**	**GIC**
$[Ru(NH_3)_6]^{3+/2+}$	[a]	$3.7(\pm 0.1)\times10^{-3}$	[b]	$3.6 (\pm 0.2)\times10^{-3}$
$[Fe(CN)_6]^{3-/4-}$	$3.2 (\pm 0.1)\times10^{-2}$	$3.1 (\pm 0.2)\times10^{-6}$	[b]	7.4×10^{-5}

[a]Reversible limit at 50 mV s^{-1}.

[b]Diffusion controlled. Where it was the case, the following diffusion coefficients were employed: $[Ru(NH_3)_6]^{3+}$ and $[Ru(NH_3)_6]^{2+}$, 7.0×10^{-6} cm^2s^{-1}; $[Fe(CN)_6]^{4-}$, 6.7×10^{-6} cm^2s^{-1}; $[Fe(CN)_6]^{3-}$ 7.6×10^{-6} cm^2s^{-1}.

by using microscale electrochemical techniques, it was shown that fast kinetics can occur on both basal and step edges, and that HOPG history does affect the ET process.[38] For instance, it was reported that extended exposure of the HOPG to the ambient environment or repeated CVs strongly decreased the heterogeneous electron transfer kinetics, compared to a freshly exfoliated HOPG.[38] This was especially true when using the $[Fe(CN)_6]^{3-/4-}$ system. Instead, with the $[Ru(NH_3)_6]^{3+/2+}$ redox couple, high values of k^0 (even higher than 0.1 cm s^{-1}) at pristine HOPG have been reported.[58] However, also with the latter redox couple, treatments or long-term exposure to the ambient environment of the HOPG sample resulted in a decrease the activity/conductivity.[38] Therefore, from the results shown in Table 2, it can be concluded that while the pristine HOPG investigated here behaves essentially as a metallic substrate and provide fast RT kinetics, the intercalation process led to sensible deterioration of conductivity, although this is most evident for the $[Fe(CN)_6]^{3-/4-}$. As for the marked difference on the ET found with the $[Fe(CN)_6]^{3-/4-}$, it was conceivably due to the surface adsorption of material on the HOPG surface (i.e., Prussian blue),[38] which somehow further passivates the surface.

3.3 | SECM characterisation

In order to obtain spatial resolved information on conductivity of the samples, SECM measurements were performed in feedback mode. As illustrated in the scheme in Section S3 of SI, the microelectrode tip was biased at a potential at which the reduction or oxidation of the redox mediators occurred under diffusion control, while the substrate was either unbiased or biased at different potentials. Typical approach curves recoded above the unbiased pristine HOPG, and, for control, above the insulating Teflon surface surrounding the sample, with both $[Fe(CN)_6]^{4-}$ and $[Ru(NH_3)_6]^{3+}$, are shown in Figure 4A. As is evident, above the insulating material, negative feedback is observed with both redox mediators (cyan and orange lines), due to the inhibition of the mass transfer towards the surface of the microelectrode, and fits the theory for a diffusion-controlled process (black line).[26] Instead, above the pristine and just exfoliated HOPG, positive feedback (blue and red lines), overlapping the theoretical diffusion-controlled response (black line), is observed. Similar approach curves were recorded in different zones of the HOPG surface. Furthermore, the 1D and 2D scans (Figure 4B,C, respectively), which allowed larger areas of the samples surface and homogeneity to be imaged, provided similar information. These results therefore indicate that the pristine HOPG behaves as a metal electrode (e.g., Au and Pt) at which positive feedback at the unbiased substrate occurs through lateral ET,[26] and are consistent with the results obtained by CV.

Similar SECM measurements, performed above the unbiased GIC substrate, displayed different results, which also depended on the redox system employed. As is shown in Figure 5A, $[Ru(NH_3)_6]^{3+/2+}$ exhibited both positive and attenuated negative feedback responses, upon varying the location of the sample investigated. Instead, $[Fe(CN)_6]^{3-/4-}$ provided only negative feedback at any location of the surface investigated. These results indicated that the intercalation process led to passivation of the HOPG surface, although it has less influence on $[Ru(NH_3)_6]^{3+/2+}$. A similar different behaviour of the two redox couples has been reported in the literature[38] and was explained as due, in part, to the faster ET kinetics of the $[Ru(NH_3)_6]^{3+/2+}$ system compared to that of $[Fe(CN)_6]^{3-/4-}$; in part, also due to possible adsorption of the latter redox probe onto the HOPG surface and even to the formation of passivating Prussian blue.[38]

In order to address how the intercalation process affected quantitatively the heterogeneous ET process, series of measurements were performed with the two redox mediators above the GIC sample biased at different potentials. Family of approach curves recorded with the two redox mediators are shown in Figure 6A,B.

As is evident, positive feedback is observed for the $[Ru(NH_3)_6]^{3+/2+}$ system with application of even small overpotentials, almost achieving the diffusion-controlled behaviour at higher overpotentials. This indicates a rather fast regeneration of the redox mediator and the occurrence of fast kinetics at the substrate. Instead, for the $[Fe(CN)_6]^{3-/4-}$ probe, rather high overpotentials are

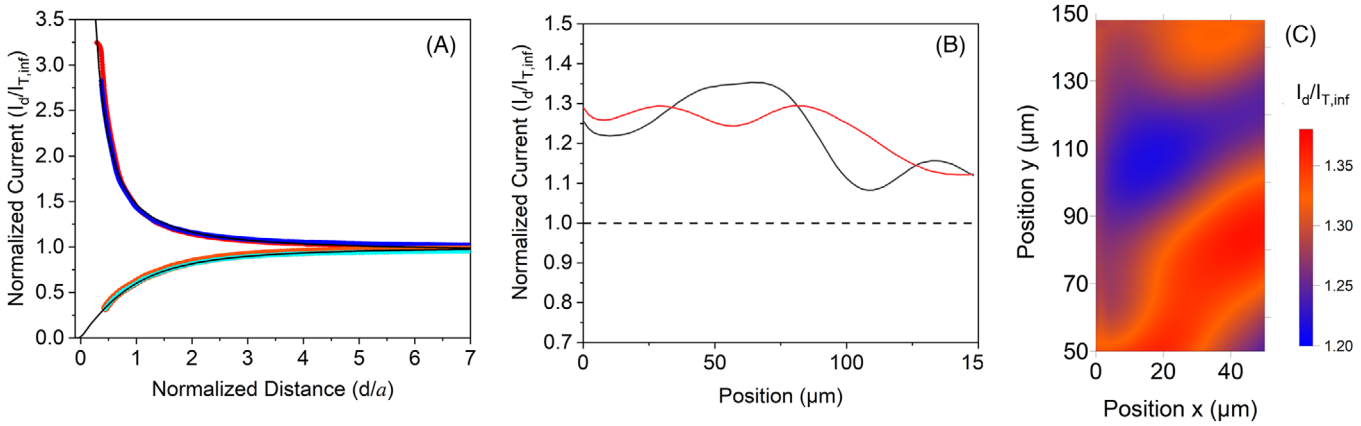

FIGURE 4 (A) Approach curves recorded using a Pt microdisk electrode (a = 12.5 μm, RG = 5) above the unbiased pristine HOPG sample in a solution containing 1 mM $[Fe(CN)_6]^{4-}$ + 0.1 M KCl (blue) or 1 mM $[Ru(NH_3)_6]^{3+}$ + 0.1 M KCl (red); for comparison the approach curves recorded above the insulating substrate with both redox mediators are shown (cyan and orange for $[Fe(CN)_6]^{4-}$ and $[Ru(NH_3)_6]^{3+}$, respectively). Black lines are theoretical approach curves for diffusion-controlled positive and negative feedback. (B, C) 1D and 2D scans above the unbiased HOPG substrate obtained in 1 mM $[Ru(NH_3)_6]^{3+}$ and a tip to-substrate distance of 12.5 μm.

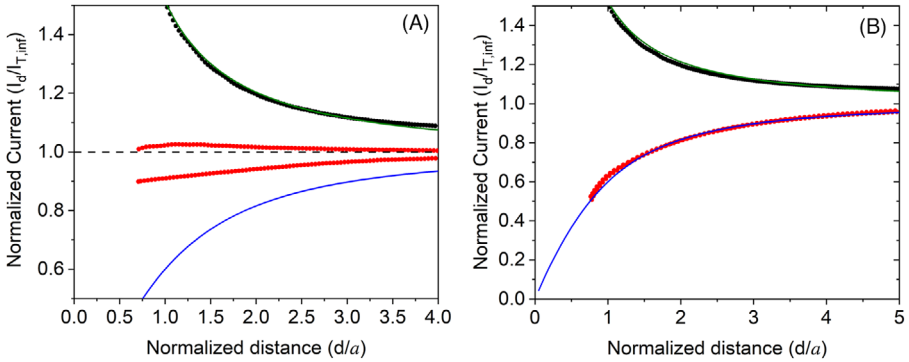

FIGURE 5 Approach curves recorded in different locations using a Pt microdisk electrode (a = 12.5 μm, RG = 5) above the unbiased GIC substrate in a solution containing 1 mM $[Ru(NH_3)_6]^{3+}$ + 0.1 M KCl (A) and 1 mM $[Fe(CN)_6]^{4-}$ + 0.1 M KCl (B), red dots; for comparison, the corresponding approach curves recorded above HOPG substrate are reported (green dots). Blue lines for theoretical diffusion-controlled positive and negative feedback.

required to obtain positive feedback, which however never achieves the diffusion-controlled behaviour. This result indicates the occurrence of slow regeneration of the redox mediator, due to slow kinetics at the substrate. These results, again, are consistent with those obtained by CVs, although the latter reflect an average surface condition.

Theory exists to obtain quantitative kinetic information by SECM. In particular, analytical relationships were derived for both negative and positive feedback approach curves for a range of SECM tips with various RG and L.[59,60] The shape of the approach curves depends on the dimensionless parameter Λ, defined as:

$$\Lambda = \frac{k \cdot a}{D}. \tag{5}$$

In this equation, k depends on the overpotential and is related to k^0 as described by the Butler–Volmer type model:[50]

$$\ln(\Lambda) = \ln(\Lambda_0) - \alpha \cdot \frac{RT}{nF} \cdot \left(E - E^{0'}\right), \tag{6}$$

where the symbols have their usual meaning. The fit of experimental and theoretical approach curves allows obtaining Λ values for a range of overpotentials $(E - E^{0'})$. Figure 6A,B with symbols shows that a good fit was obtained for both redox mediators. Relevant Λ value thus obtained were used to construct the plots of ln(Λ) versus $(E - E^{0'})$ shown (Figure 6C,D). The linear regression analysis of experimental points provided the following relationships:

$$\ln(\Lambda) = 18.96(E - E^{0'}) - 0.44$$

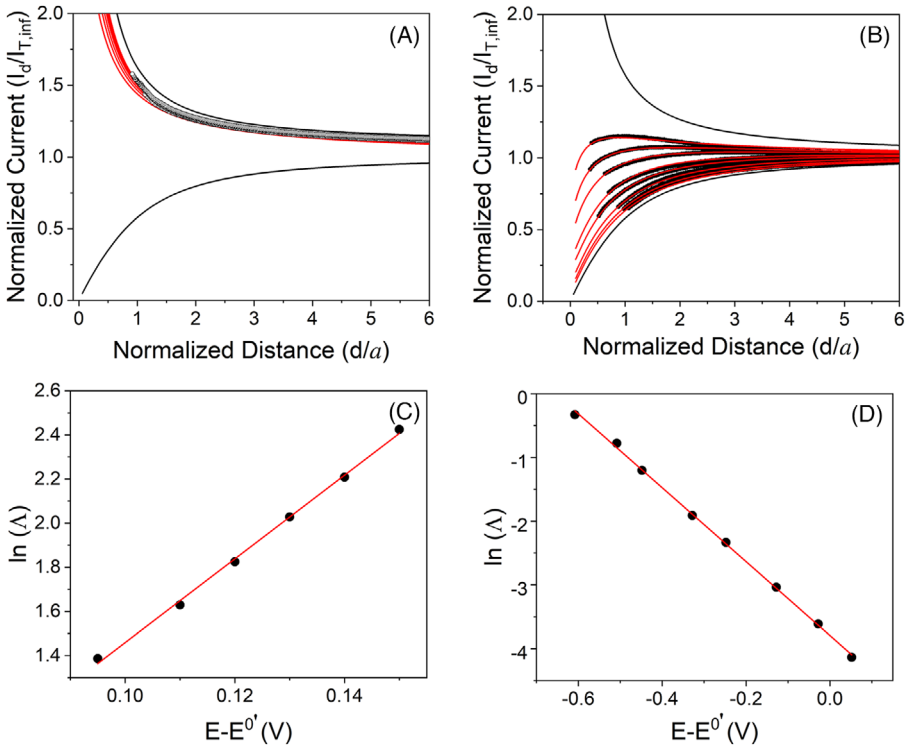

FIGURE 6 Experimental approach curves recorded in a solution containing: (A) 1 mM $[Ru(NH_3)_6]^{3+}$ + 0.1 M KCl, applying E_{tip} = −0.3 V vs. Ag/AgCl and varying the potential of the substrate (E_{sub} = −0.065, −0.050, 0.220, 0.040, −0.030, −0.020, −0.010, +0.000 V vs. Ag/AgCl; empty dots). (B) 1 mM $[Fe(CN)_6]^{4-}$, + 0.1 M KCl supporting electrolyte, applying E_{tip} = +0.4 V vs. Ag/AgCl and varying the potential of the substrate (E_{sub} = −0.380, −0.280, 0.220, 0.100, −0.020, +0.100, +0.200 V vs. Ag/AgCl; empty dots). The SECM tip was a Pt microdisk electrode 12.5 μm radius and RG = 5. Theoretical approach curves obtained from Refs. (59 and 60) (red lines) and diffusion-controlled positive and negative feedback approach curves (black full lines). (C, D) The analysis of ln Λ vs. ($E - E^{0'}$), by fitting experimental and theoretical approach curves obtained using $[Ru(NH_3)_6]^{3+}$ and $[Fe(CN)_6]^{4-}$, respectively.

and

$$\ln(\Lambda) = -5.80(E - E^{0'}) - 4.43$$

for the $[Ru(NH_3)_6]^{3+/2+}$ and $[Fe(CN)_6]^{3/4-}$ system, respectively.

From Equation (5) and considering the diffusion coefficients of $[Ru(NH_3)_6]^{2+}$ (7.0×10^{-6} cm^2 s^{-1})[40] and $[Fe(CN)_6]^{3-}$ (7.6×10^{-6} cm^2 s^{-1}),[50] that is, the species being involved in the redox process at the substrate, k^0 values shown in Table 2 (second column) were obtained. The values found by SECM are close to those found by CV for the $[Ru(NH_3)_6]^{3+/2+}$ system. Instead, for the $[Fe(CN)_6]^{3-/4-}$ system, k^0 values are larger (about an order of magnitude) compared to those found by CV (Table 2). The larger value can be explained by considering that the theoretical approach curves employed are sufficiently accurate for $\Lambda \geq 0.01$.[59,60] On the basis of k^0 found by CV and considering Equation (5), for the $[Fe(CN)_6]^{3-/4-}$ system, $\Lambda << 0.01$. Therefore, the k^0 value found by SECM for the latter system can be considered as an upper limit of the ET kinetics. Instead for the $[Ru(NH_3)_6]^{3+/2+}$ system the Λ value equal to 0.6 falls well in the range 0.01–10 of validity of the theoretical equations employed to fit theoretical and experimental approach curves.[59,60]

Beyond the considerations set above, some discrepancies between ET kinetics found by CV and SECM may arise from the fact that while CV provides average information for the entire surface examined, SECM furnishes information on smaller surface areas, thus highlighting some heterogeneity of the conductivity/activity across the surface. This is especially true for the HOPG intercalated sample. To get insights on the latter aspect and also to confirm that the intercalated HOPG was less electrochemical active compared to the pristine material, 1D and 2D SECM scans were performed at the boundary of an HOPG sample intercalated for only half of its surface. These measurements were performed by using the $[Ru(NH_3)_6]^{3+/2+}$ system, which is less affected by surface deterioration due to eventual adsorption or other surface passivation phenomena. Figure 7 shows typical 1D and 2D images thus obtained. As is evident, a sharp drop of the normalised current occurs when the tip from the pristine HOPG reaches the intercalated zone. This

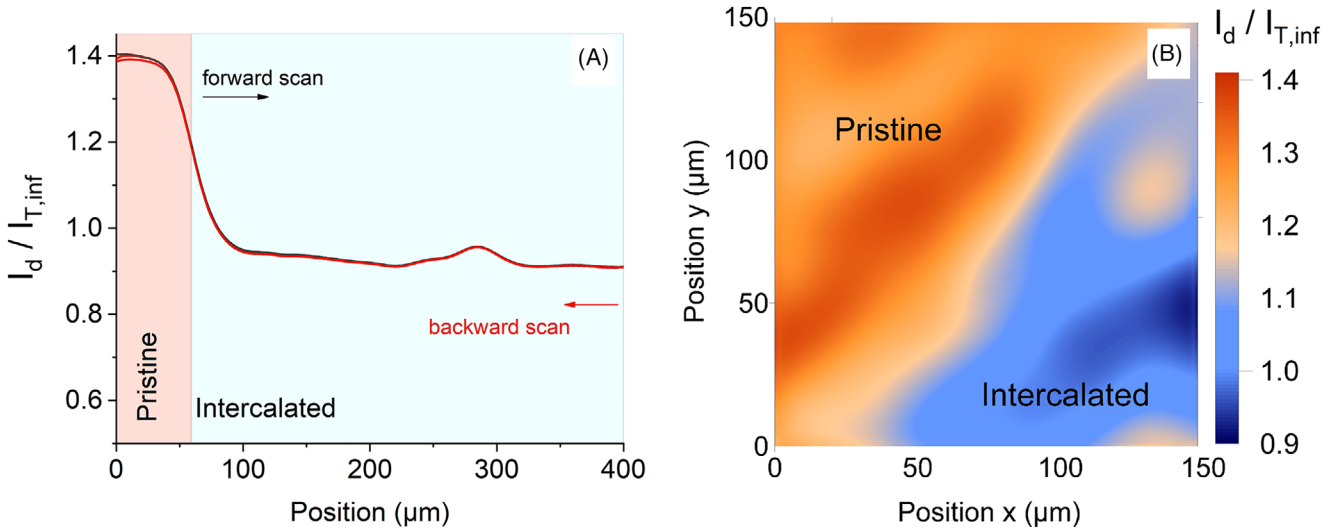

FIGURE 7 1D (A) and 2D (B) scans recorded with a Pt microdisk electrode ($a = 12.5$ μm; $RG = 5$) positioned 12 μm above the surface at the boundary between the pristine and intercalated HOPG sample. Measurements performed in a solution containing 1 mM $[Ru(NH_3)_6]^{3+}$ + 0.1 M KCl. The tip was biased at –0.3 V vs. Ag/AgCl, while the substrate was unbiased. Arrows indicated the scan direction in the 1D scan: forward (black) and backward (red).

trend is reproducible as was verified by performing 1D scan in the forward and backward directions (black and red lines). Both images are consistent with the transition from a more active to a less active zone. In addition, above the GIC surface, local heterogeneity in the activity can be observed as indicated by the small humps with higher normalised currents. A similar level of heterogeneity was also recorded above the pristine HOPG over a scale of (50×150) μm^2 (Figure 4B,C) and this can be attributed to an intrinsic variability of the activity of the pristine HOPG surface, due to crystallographic properties of the sample, such as the mosaic spread, and related topological/structural characteristics (see the bulges and hollows of Figure S1 of SI).

However, the results obtained by both CV and SECM, overall, indicate that the conductivity, and consequently the electrochemical behaviour of intercalated HSO_4^- and SO_4^{2-} HOPG samples is quite different from the pristine material.

It must be considered that the SECM tip employed here, although provided some spatial resolved information on the heterogeneity of the surface conductivity, reflects also changes in the surface topography.[26,27,32] A way to surmount the overlapping information is the use of the combined SECM-AFM technique,[58,61,62] which allows the deconvolution of the responses related to topography and conductivity/reactivity of the sample and, at the same time, provides much higher spatial resolution. Work in this direction on anions-intercalated HOPG is ongoing in our laboratory.

4 | CONCLUSION

In this paper, the effect of the electrochemical intercalation of HSO_4^- and SO_4^{2-} in HOPG samples on the conductivity of the pristine material has been investigated using the microscopic techniques of AFM and SECM, together with CV, the latter providing macroscopic information. In particular, the ET kinetics of both pristine and intercalated HOPG have been studied by using the redox systems $[Ru(NH_3)_6]^{3+/2+}$ and $[Fe(CN)_6]^{3-/4-}$. The results indicated that the conductivity and, consequently, the ET kinetic of the intercalated samples is diminished, compared to the pristine one. However, the extent of the ET decrease markedly depended on the redox couple employed, and it was larger for the $[Fe(CN)_6]^{3-/4-}$ system. SECM images obtained by using $[Ru(NH_3)_6]^{3+/2+}$ evidenced some heterogeneity in the surface activity, while AFM images revealed a profound change in surface topography. Overall, the preliminary results reported in this work suggest that a correlation exists between electrochemical activity and crystallographic/topographic characteristics of the materials. However, to put on quantitative basis this correlation, the intercalation of the HPOG and its subsequent characterisation by both AFM and SECM need to be performed adopting an approach in which all steps, that is, electrochemical intercalation, AFM and SECM characterisation of the HOPG are performed in the same cell and apparatus. Moreover, the spatial resolution of both AFM and SECM (essentially related to the tip size) should be made comparable. In perspective, working with an operando system

based on the use of an AFM-SECM probe shall overcome the above limitation.

AUTHOR CONTRIBUTIONS

The manuscript was written through contributions of all authors. All authors have given approval to the final version of the manuscript.

ACKNOWLEDGEMENTS

The experiments of EC intercalation and AFM have been performed at the Solid-Liquid Interface Nanomicroscopy and Spectroscopy laboratory (SoLINano-∑ LAB, https://www.polimi.it/en/research/laboratories/interdepartmental-laboratories/solinano-s-lab-solid-liquid-interface-nanomicroscopy-and-spectroscopy-lab) which is an interdepartmental facility at Politecnico di Milano.

ORCID

Rossella Yivlialin https://orcid.org/0000-0002-6824-1519
Gianlorenzo Bussetti https://orcid.org/0000-0001-8556-8014
Salvatore Daniele https://orcid.org/0000-0003-0315-1819

REFERENCES

1. Besenhard, J. O., & Fritz, H. P. (1983). The Electrochemistry of black carbons. *Angewandte Chemie—International Edition English*, *22*(12), 950–975. https://doi.org/10.1002/anie.198309501
2. Lincoln Vogel, F. (1977). The electrical conductivity of graphite intercalated with superacid fluorides: experiments with antimony pentafluoride. *Journal of Materials Science*, *12*, 982–986.
3. Forsman, W. C., Vogel, F. L., Carl, D. E., & Hoffman, J. (1978). Chemistry of graphite intercalation by nitric acid. *Carbon N. Y.*, *16*(4), 269–271. https://doi.org/10.1016/0008-6223(78)90040-4
4. Pietronero, L., & Tosatti, E. (1981). Physics of intercalation compounds. In *Proceedings of an International Conference Trieste*. Springer Verlag Berlin Heidelberg New York, Berlin.
5. McRae, E., & Mareche, J. F. (1985). Stage dependence of the electrical resistivity of graphite intercalation compounds. *Journal of Physics C: Solid State Physics*, *18*(8), 1627–1640. https://doi.org/10.1088/0022-3719/18/8/010
6. Foley, G. M. T., Zeller, C., Falardeau, E. R., & Vogel, F. L. (1977). Room temperature electrical conductivity of a highly two dimensional synthetic metal: AsF5-graphite. *Solid State Communications*, *24*(47), 423–428.
7. Yamada, Y., Miyazaki, K., & Abe, T. (2010). Role of edge orientation in kinetics of electrochemical intercalation of lithium-ion at graphite. *Langmuir*, *26*(18), 14990–14994. https://doi.org/10.1021/la1019857
8. Tongay, S., Hwang, J., Tanner, D. B., Pal, H. K., Maslov, D., & Hebard, A. F. (2010). Supermetallic conductivity in bromine-intercalated graphite. *Physical Review B: Condensed Matter and Materials Physics*, *81*(11), 1–6. https://doi.org/10.1103/PhysRevB.81.115428
9. Park, S., & Ruoff, R. S. (2009). Chemical methods for the production of graphenes. *Nature Nanotechnology*, *4*(4), 217–224. https://doi.org/10.1038/nnano.2009.58
10. Metrot, A., & Fischer, J. E. (1981). Charge transfer reactions during anodic oxidation of graphite in H2SO4. *Synthetic Metals*, *3*(3–4), 201–207. https://doi.org/10.1016/0379-6779(81)90009-6
11. Touhara, H., Goto, Y., Watanabe, N., Imaeda, K., Enoki, T., Inokuchi, H., & Mizutani, Y. (1988). Fluorine-graphite HOPG intercalation compounds. *Synthetic Metals*, *23*(1–4), 461–466. https://doi.org/10.1016/0379-6779(88)90522-X
12. Harrach, A., Nicollin, C., & Metrot, A. (1989). In-plane conductivity of electrochemically intercalated pyrographite. *Synthetic Metals*, *34*, 467–472.
13. Castro Neto, A. H., Guinea, F., Peres, N. M. R., Novoselov, K. S., & Geim, A. K. (2009). The electronic properties of graphene. *Review of Modern Physics*, *81*(1), 109–162. https://doi.org/10.1103/RevModPhys.81.109
14. Xia, Z., Bellani, V., Sun, J., & Palermo, V. (2021). Electrochemical exfoliation of graphite in H2SO4, Li2SO4 and NaClO4 solutions monitored: In situ by Raman microscopy and spectroscopy. *Faraday Discussions*, *227*, 291–305. https://doi.org/10.1039/c9fd00123a
15. Yivlialin, R., Bussetti, G., Duò, L., Yu, F., Galbiati, M., & Camilli, L. (2018). CVD graphene/Ni interface evolution in sulfuric electrolyte. *Langmuir*, *34*(11). https://doi.org/10.1021/acs.langmuir.8b00459
16. Gutman, D. B., Tongay, S., Pal, H. K., Maslov, D. L., & Hebard, A. F. (2009). Graphite in the bilayer regime: In-plane transport. *Physical Review B: Condensed Matter and Materials Physics*, *80*(4), 1–5. https://doi.org/10.1103/PhysRevB.80.045418
17. Vogel, F. L., Fuzellier, H., Zeller, C., & McRae, E. J. (1979). In-plane electrical resistivity of nitric acid intercalated graphite. *Carbon N. Y.*, *17*(3), 255–257. https://doi.org/10.1016/0008-6223(79)90084-8
18. Pietronero, L., Strässler, S., Zeller, H. R., & Rice, M. J. (1980). Electrical conductivity of a graphite layer. *Physical Review B*, *22*(2), 904, https://doi.org/10.1103/PhysRevB.22.904
19. Fischer, J. E., & Thompson, T. E. (1978). Graphite intercalation compounds. *Physics Today*, *31*(7), 36–45. https://doi.org/10.1063/1.2995104
20. Hathcock, K. W., Brumfield, J. C., Goss, C. A., Irene, E. A., & Murray, R. W. (1995). Incipient Electrochemical oxidation of highly oriented pyrolytic graphite: Correlation between surface blistering and electrolyte anion intercalation. *Analytical Chemistry*, *67*(13), 2201–2206. https://doi.org/10.1021/ac00109a045
21. Goss, C. A., Brumfield, J. C., Irene, E. A., & Murray, R. W. (1993). Imaging the incipient electrochemical oxidation of highly oriented pyrolytic graphite. *Analytical Chemistry*, *65*(10), 1378–1389. https://doi.org/10.1021/ac00058a014
22. Bussetti, G., Yivlialin, R., Alliata, D., Li Bassi, A., Castiglioni, C., Tommasini, M., Casari, C. S., Passoni, M., Biagioni, P., Ciccacci, F., & Duò, L. (2016). Disclosing the early stages of electrochemical anion intercalation in graphite by a combined atomic force microscopy/scanning Tunneling microscopy approach. *Journal of Physical Chemistry C*, *120*(11). https://doi.org/10.1021/acs.jpcc.6b00407
23. Yivlialin, R., Brambilla, L., Accogli, A., Gibertini, E., Tommasini, M., Goletti, C., Leone, M., Duò, L., Magagnin, L., Castiglioni, C., & Bussetti, G. (2020). Evidence of graphite blister

evolution during the anion de-intercalation process in the cathodic regime. *Applied Surface Science*, 504. https://doi.org/10.1016/j.apsusc.2019.144440

24. Aneja, K. S., Böhm, H. L. M., Khanna, A. S., & Böhm, S. (2017). Functionalised graphene as a barrier against corrosion. *FlatChem*, *1*, 11–19. https://doi.org/10.1016/j.flatc.2016.08.003
25. You, R., Liu, Y. Q., Hao, Y. L., Han, D. D., Zhang, Y. L., & You, Z. (2020). Laser fabrication of graphene-based flexible electronics. *Advanced Materials*, *32*(15), 1–22. https://doi.org/10.1002/adma.201901981
26. Bard, A. J., & Mirkin, M. V. (2022). Scanning electrochemical microscopy. CRC Press: Boca Raton. https://doi.org/10.1201/9781003004592
27. Daniele, S., & Denuault, G. (2014). From microelectrodes to scanning electrochemical microscopy. In Pletcher D., Tian Z.-Q., & Williams D. E. (Eds.), *Developments in electrochemistry: Science inspired by Martin Fleishmann*. Wiley. https://doi.org/10.1002/9781118694404.ch12
28. Polcari, D., Dauphin-Ducharme, P., & Mauzeroll, J. (2016). Scanning electrochemical microscopy: A comprehensive review of experimental parameters from 1989 to 2015. *Chemical Reviews*, *116*(22), 13234–13278. https://doi.org/10.1021/acs.chemrev.6b00067
29. Polcari, D., Dauphin-Ducharme, P., & Mauzeroll, J. (2016). Scanning electrochemical microscopy: A comprehensive review of experimental parameters from 1989 to 2015. *Chemical Reviews*, *116*(22), 13234–13278. https://doi.org/10.1021/acs.chemrev.6b00067
30. Baldi, F., Daniele, S., Gallo, M., Paganelli, S., Battistel, D., Piccolo, O., Faleri, C., Puglia, A. M., & Gallo, G. (2016). Polysaccharide-based silver nanoparticles synthesized by *Klebsiella oxytoca* DSM 29614 cause DNA fragmentation in *E. coli* cells. *Biometals*, *29*(2), 321–331. https://doi.org/10.1007/s10534-016-9918-4
31. Battistel, D., Baldi, F., Gallo, M., Faleri, C., & Daniele, S. (2015). Characterisation of biosynthesised silver nanoparticles by scanning electrochemical microscopy (SECM) and voltammetry. *Talanta*, *132*, 294–300. https://doi.org/10.1016/j.talanta.2014.09.023
32. Santana Santos, C., Jaato, B. N., Sanjuán, I., Schuhmann, W., & Andronescu, C. (2023). Operando scanning electrochemical probe microscopy during electrocatalysis. *Chemical Reviews*, *123*(8), 4972–5019. https://doi.org/10.1021/acs.chemrev.2c00766
33. Hui, J., Burgess, M., Zhang, J., & Rodríguez-López, J. (2016). Layer number dependence of Li+ intercalation on few-layer graphene and electrochemical imaging of its solid-electrolyte interphase evolution. *ACS Nano*, *10*(4), 4248–4257. https://doi.org/10.1021/acsnano.5b07692
34. Santana, J. J., Izquierdo, J., & Souto, R. M. (2022). Uses of scanning electrochemical microscopy (SECM) for the characterization with spatial and chemical resolution of thin surface layers and coating systems applied on metals: A review. *Coatings*, *12*(5). https://doi.org/10.3390/coatings12050637
35. Bonazza, G., Girault, H. H., Lesch, A., & Daniele, S. (2023). Simultaneous local sensing of two chemical properties with dual soft probe scanning electrochemical microscopy. *Electrochimica Acta*, *462*, 142752. https://doi.org/10.1016/j.electacta.2023.142752
36. Mishra, A., Sarbapalli, D., Rodríguez, O., & Rodríguez-López, J. (2023). electrochemical imaging of interfaces in energy storage via scanning probe methods: Techniques, applications, and prospects. *Annual Review of Analytical Chemistry*, *16*, 93–115. https://doi.org/10.1146/annurev-anchem-091422-110703
37. Zhang, G., Cuharuc, A. S., Güell, A. G., & Unwin, P. R. (2015). Electrochemistry at highly oriented pyrolytic graphite (HOPG): Lower limit for the kinetics of outer-sphere redox processes and general implications for electron transfer models. *Physical Chemistry Chemical Physics*, *17*(17), 11827–11838. https://doi.org/10.1039/c5cp00383k
38. Patel, A. N., Collignon, M. G., O'connell, M. A., Hung, W. O. Y., Mckelvey, K., Macpherson, J. V., & Unwin, P. R. (2012). A new view of electrochemistry at highly oriented pyrolytic graphite. *Journal of the American Chemical Society*, *134*(49), 20117–20130. https://doi.org/10.1021/ja308615h
39. Saito, Y. (1951). A theoretical study on the diffusion current at the stationary electrodes of circular and narrow band types. *Review of Polarography*, *1968*, 15.
40. Battistel, D., Pecchielan, G., & Daniele, S. (2014). Micropipette contact technique as a tool to reveal, characterize, and modify nanopore electrodes. *ChemElectroChem*, *1*(1), 140–146. https://doi.org/10.1002/celc.201300147
41. De Rosa, S., Branchini, P., Spampinato, V., Franquet, A., Yivlialin, R., Duò, L., Bussetti, G., & Tortora, L. (2022). Stratigraphic analysis of intercalated graphite electrodes in aqueous inorganic acid solutions. *Nano Research*, *15*(2), 1120–1127. https://doi.org/10.1007/s12274-021-3614-6
42. Legrand, A. P., & Flandrois, S. (1987). *Chemical physics of intercalation* (1st ed.). New York, NY: Springer.
43. Pavoni, E., Yivlialin, R., Hardly Joseph, C., Fabi, G., Mencarelli, D., Pierantoni, L., Bussetti, G., & Farina, M. (2019). Blisters on graphite surface: A scanning microwave microscopy investigation. *RSC Advances*, *9*(40), 23156–23160. https://doi.org/10.1039/c9ra04667d
44. Bussetti, G., Yivlialin, R., Goletti, C., Zani, M., & Duò, L. (2019). Temperature effects on the Hopg intercalation process. *Condensed Matter*, *4*(1), 1–6. https://doi.org/10.3390/condmat4010023
45. Bussetti, G., Yivlialin, R., Ciccacci, F., Duò, L., & Podestà, A. (2024). *Blistering at the solid-liquid interface: The graphite case-study*. In Wandelt, K., & Bussetti, G. (Eds.), *Encyclopedia of solid-liquid interfaces*. Elsevier.
46. Menegazzo, M., Marfori, L., Yivlialin, R., Podestà, A., Ciccacci, F., Duò, L., Russo, V., Campione, M., & Bussetti, G. (2024). Stiffness and mechanical manipulation of blisters grown on electrochemically intercalated graphite. *Electrochimica Acta*, 488 (January). https://doi.org/10.1016/j.electacta.2024.144201
47. Beck, F., Jiang, J., & Krohn, H. (1995). Potential oscillations during galvanostatic overoxidation of graphite in aqueous sulphuric acids. *Journal of Electroanalytical Chemistry*, *389*(1–2), 161–165. https://doi.org/10.1016/0022-0728(95)03870-M
48. Yivlialin, R., Brambilla, L., Bussetti, G., Tommasini, M., Bassi, A. L., Casari, C. S., Passoni, M., Ciccacci, F., Duò, L., & Castiglioni, C. (2016). Evolution of the graphite surface in phosphoric acid: An AFM and Raman study. *Beilstein Journal of Nanotechnology*, *7*(1). https://doi.org/10.3762/BJNANO.7.180
49. Cassidy, J. F., de Carvalho, R. C., & Betts, A. J. (2023). Use of inner/outer sphere terminology in electrochemistry—A hexacyanoferrate II/III case study. *Electrochem*, *4*(3), 313–349. https://doi.org/10.3390/electrochem4030022

50. Bard, A. J., & Faulkner, L. R. (2001). Electrochemical methods. In D. Harris, & E. Swain (Eds.), *Fundamentals and applications* (2nd ed.). New York: John Wiley & Sons, Ltd.
51. Nicholson, R. S., & Shain, I. (1964). theory of stationary electrode polarography: Single scan and cyclic methods applied to reversible, irreversible, and kinetic systems. *Analytical Chemistry*, *36*(7), 1212. https://doi.org/10.1021/ac60213a053
52. Lavagnini, I., Antiochia, R., & Magno, F. (2004). An extended method for the practical evaluation of the standard rate constant from cyclic voltammetric data. *Electroanalysis*, *16*(6), 505–506. https://doi.org/10.1002/elan.200302851
53. Klingler, R. J., & Kochi, J. K. (1981). Electron-transfer kinetics from cyclic voltammetry. quantitative description of electrochemical reversibility. *Journal of Physical Chemistry*, *85*(12), 1731–1741. https://doi.org/10.1021/j150612a028
54. Kneten, K. R., & McCreery, R. L. (1992). Effects of redox system structure on electron-transfer kinetics at ordered graphite and glassy carbon electrodes. *Analytical Chemistry*, *64*(21), 2518–2524. https://doi.org/10.1021/ac00045a011
55. Lee, C. Y., Guo, S. X., Bond, A. M., & Oldham, K. B. (2008). Effect of heterogeneity on the DC and AC voltammetry of the [Fe(CN)6]3-/4- solution-phase process at a highly ordered pyrolytic graphite electrode. *Journal of Electroanalytical Chemistry*, *615*(1), 1–11. https://doi.org/10.1016/j.jelechem.2007.11.029
56. Banks, C. E., & Compton, R. G. (2006). New electrodes for old: from carbon nanotubes to edge plane pyrolytic graphite. *Analyst*, *131*(1), 15–21. https://doi.org/10.1039/b512688f
57. Nwamba, O. C., Echeverria, E., McIlroy, D. N., Austin, A., Shreeve, J. M., & Aston, D. E. (2019). Thermal modification of graphite for fast electron transport and increased capacitance. *ACS Applied Nano Materials*, *2*(1), 228–240. https://doi.org/10.1021/acsanm.8b01887
58. Lai, S. C. S., Patel, A. N., McKelvey, K., & Unwin, P. R. (2012). Definitive evidence for fast electron transfer at pristine basal plane graphite from high-resolution electrochemical imaging. *Angewandte Chemie—International Edition*, *51*(22), 5405–5408. https://doi.org/10.1002/anie.201200564
59. Cornut, R., & Lefrou, C. (2008). New analytical approximation of feedback approach curves with a microdisk SECM tip and irreversible kinetic reaction at the substrate. *Journal of Electroanalytical Chemistry*, *621*(2), 178–184. https://doi.org/10.1016/j.jelechem.2007.09.021
60. Cornut, R., Griveau, S., & Lefrou, C. (2010). Accuracy study on fitting procedure of kinetics SECM feedback experiments. *Journal of Electroanalytical Chemistry*, *650*(1), 55–61. https://doi.org/10.1016/j.jelechem.2010.09.007
61. Watkins, T. S., Sarbapalli, D., Counihan, M. J., Danis, A. S., Zhang, J., Zhang, L., Zavadil, K. R., & Rodríguez-López, J. (2020). A combined SECM and electrochemical AFM approach to probe interfacial processes affecting molecular reactivity at redox flow battery electrodes. *Journal of Materials Chemistry A*, *8*(31), 15734–15745. https://doi.org/10.1039/d0ta00836b
62. Daboss, S., Rahmanian, F., Stein, H. S., & Kranz, C. (2022). The potential of scanning electrochemical probe microscopy and scanning droplet cells in battery research. *Electrochemical Science Advances*, *2*(4), 1–10. https://doi.org/10.1002/elsa.202100122

SUPPORTING INFORMATION

Additional supporting information can be found online in the Supporting Information section at the end of this article.

How to cite this article: Yivlialin, R., Bonazza, G., Battistel, D., Bussetti, G., & Daniele, S. (2025). Macroscopic and microscopic electron transfer kinetics of HOPG and graphite intercalated compound investigated by cyclic voltammetry and SECM. *Journal of Microscopy*, 1–13. https://doi.org/10.1111/jmi.13435